ÆPTIC: JOURNAL OF PLASMA, BIOELECTRICS & EVOLUTIONARY SCIENCE

ÆPTIC (2026) 2:1 | Articles | DOI: 10.64916/aeptic.v2i1.001

Planetary Bioelectromagnetic Coherence: A Phase-Field Framework for Earth–Life Coupling and Phase Instability

Doha Lee
DohaTesla Lab, South Korea
doha.lee@dohateslalab.org

Received: January 10, 2026 | **Accepted:** March 5, 2026 | **Published online:** March 23, 2026 | Open Access

Abstract

Human–environment systems operate as coupled bioelectromagnetic networks exhibiting phase dynamics across biological, ecological, and geophysical domains. This study introduces a phase-field framework to characterize systemic coherence in terms of phase alignment ($\Delta\phi$), coupling strength (κ), and informational gradient (∇I). Using cross-domain observational datasets—including heart-rate variability under light exposure, behavioral responses of magnetosensitive species during geomagnetic disturbances, and environmental electromagnetic variability—we identify recurring patterns associated with changes in system-level coherence.

Across these domains, increasing phase deviation ($\Delta\phi$) is frequently observed to be associated with reduced coupling strength (κ) and elevated informational gradients (∇I), suggesting a possible common structure of coherence degradation. Rather than relying on controlled experimental isolation, the framework interprets naturally occurring environmental perturbations as observable phase inputs within a coupled Earth–life system.

Within this formulation, ecological resilience may be interpreted as a function of bioelectromagnetic coherence. The proposed framework provides a quantitative, theory-driven basis for analyzing stability and disruption across interconnected planetary systems, supported by cross-domain observational evidence.

Keywords: Phase-field model; Bioelectromagnetic coherence; Earth–life coupling; Phase synchronization; Geomagnetic interaction

1 Introduction

Human–environment systems can be understood as interacting processes influenced by electromagnetic, optical, and mechanical factors across multiple spatial and temporal scales. Over the past century, large-scale technological developments have altered environmental conditions in ways that may affect the coupling between biological oscillatory systems and geophysical fields. Artificial illumination, power transmission networks, and land-use modification have been associated with changes in environmental electromagnetic structure, with potential implications for biological synchronization processes.

Conventional environmental studies have primarily interpreted these changes in terms of chemical pollution or biodiversity loss. However, recent work suggests that environmental variability in frequency, phase, and field conditions may also influence biological regulation. For example, nocturnal light exposure has been shown to affect melatonin secretion and autonomic balance, and may be associated with measurable phase differences ($\Delta\phi$) between physiological oscillators such as cardiac and neural rhythms. Phase synchronization is known to contribute to large-scale neural and physiological integration [1], providing a relevant biological context for examining coherence-related dynamics.

Under natural nocturnal conditions, biological systems typically exhibit circadian patterns characterized by parasympathetic predominance and reduced environmental variability. Artificial illumination and socially imposed schedules may alter these dynamics, and have been associated with changes in heart rate variability (HRV), sleep quality, and metabolic regulation. These observations suggest that environmental perturbations can influence phase relationships within biological systems, although the mechanisms and extent of these effects remain under investigation.

In addition to localized environmental factors, large-scale anthropogenic energy releases may introduce transient perturbations in atmospheric and geomagnetic conditions. Such events have been associated with short-term variations in geomagnetic indices (e.g., Kp), as well as behavioral responses in magnetosensitive species. While the extent of global

propagation and biological impact remains uncertain, these observations motivate further investigation into the role of environmental electromagnetic variability in cross-scale system dynamics.

Within this context, this study examines the relationship between phase deviation ($\Delta\phi$), coupling strength (κ), and informational gradients (∇I) using a phase-field modeling framework. The goal is to provide a quantitative structure for analyzing how environmental perturbations may be associated with changes in system-level coherence across biological and geophysical domains.

The present work is situated at the interface of biophysics and complex systems science. By integrating observational patterns across biological, atmospheric, and geomagnetic domains, the proposed framework introduces a phase-based representation that links phase deviation ($\Delta\phi$), coupling strength (κ), and informational gradients (∇I) within a unified quantitative structure for Earth–life system dynamics.

2 Methods: Quantitative Modeling Framework

2.1 Research Objective and Quantitative Model

This study defines coexistence as a measurable condition related to phase stability within a coupled Earth–life oscillator framework. In this context, coexistence is operationalized in terms of interactions among biological processes (bioelectromagnetic field), atmospheric electrical conditions (atmospheric charge structure), and geomagnetic variability (geomagnetic flux). Rather than focusing solely on material balance, this approach considers the role of phase relationships in shaping system-level stability.

Within this framework, system behavior is described using three variables: phase deviation ($\Delta\phi$), coupling strength (κ), and informational gradient (∇I). These variables provide a tractable representation of synchronization dynamics across biological and geophysical domains. In practical applications, the informational gradient (∇I) is approximated using measurable proxies such as entropy measures, signal variance, or spatial heterogeneity indices, depending on data availability and system scale, thereby enabling empirical estimation of ∇I across domains.

A stable coexistence condition is expressed as:

$$\text{Coexistence} \iff \begin{cases} \mathrm{Var}(\Delta\phi) \leq \varepsilon, \\ \dfrac{d\kappa}{dt} \approx 0, \\ \|\nabla I\| \to \min \end{cases} \tag{1}$$

where $\Delta\phi$ represents the phase difference between biological and environmental oscillators, κ denotes an effective coupling coefficient, and ∇I represents spatial variation in information-related signals across the system. Stability is interpreted as a regime in which these variables remain within bounded ranges over time.

Environmental perturbations and phase variability. Anthropogenic and environmental factors may introduce variability in phase relationships through multiple mechanisms. High-energy events can be associated with transient electromagnetic disturbances that propagate across lithospheric and ionospheric domains. Artificial nocturnal illumination has been linked to alterations in circadian timing and physiological regulation. Electrical infrastructure may influence local electromagnetic environments, while land-use changes can affect conductivity and charge exchange processes. These factors are considered as potential contributors to variability in $\Delta\phi$, κ, and ∇I.

Observable system responses. Such perturbations may be reflected in observable biological and ecological responses. Reported phenomena include changes in heart rate variability (HRV), behavioral alterations in magnetosensitive species, and large-scale ecological disturbances. These observations are examined in relation to variations in geomagnetic indices (e.g., Kp, Dst) and other environmental parameters, without assuming direct causality.

Operational definition of stability. System stability is evaluated using statistical properties of the phase variables, including $\mathrm{Var}(\Delta\phi)$, temporal variation in κ, and spatial gradients of ∇I. A stable regime is defined when $\mathrm{Var}(\Delta\phi) \leq \varepsilon$, $d\kappa/dt \approx 0$, and $\|\nabla I\|$ remains bounded. These conditions provide an operational basis for analyzing coherence-related dynamics within the model.

2.2 Analytical Scope

The analytical framework integrates datasets from biological, geomagnetic, and atmospheric domains. Geomagnetic activity indices (e.g., Kp, Dst) are analyzed alongside biological indicators such as HRV, circadian-related measures, and ecological observations. Statistical comparisons are used to examine potential associations between environmental variability and changes in biological or ecological patterns.

The analysis utilizes publicly available datasets, including geomagnetic indices (NASA OMNIWeb), satellite-based illumination data (NASA Worldview), meteorological records (KMA), seismic data (USGS), electricity usage statistics (KEPCO), and national health data (NHIS). A geospatial representation of electromagnetic exposure was constructed using infrastructure data to support spatial interpretation of urban environments.

2.3 Modeling Framework

The planetary system is modeled as a distributed phase-coupled oscillator network, in which each oscillator i evolves according to:

$$\frac{d\theta_i}{dt} = \omega_i + \kappa \sum_j W_{ij} \sin(\theta_j - \theta_i) + \alpha \nabla I_i, \tag{2}$$

where W_{ij} represents the structured coupling between bio–geo elements, and ∇I_i denotes the local information gradient driving phase adaptation. This formulation introduces an additional information-driven term and structured coupling, enabling phase dynamics that incorporate directional interactions across domains.

The interaction term represents a generalized phase-coupling structure adapted for bio–geophysical systems, rather than a specific canonical synchronization model. Here, coupling is modulated by structured interactions (W_{ij}) and directional information gradients (∇I_i), enabling cross-domain phase dynamics beyond conventional oscillator formulations.

To quantify system-level organization, global coherence (C) is defined as:

$$C = 1 - \frac{\mathrm{Var}(\Delta\phi)}{\pi^2}, \tag{3}$$

where $\mathrm{Var}(\Delta\phi)$ denotes the variance of phase differences across the oscillator ensemble. Higher values of C correspond to stronger phase alignment and reduced dispersion of oscillatory states.

Within this framework, coexistence is interpreted as a dynamically maintained regime in which phase deviations ($\Delta\phi$) remain bounded and coupling strength (κ) exhibits slow temporal variation. This provides an operational interpretation of stability in coupled biological–geophysical systems without requiring strict phase-locking conditions.

Dimensional normalization. All parameters in Eqs. (2)–(3) are expressed in dimensionless form. Phase deviation $\Delta\phi$ is measured in radians, κ is unitless, and ∇I is normalized using a reference scale proportional to B_0^2/τ_0, where τ_0 represents a characteristic timescale and B_0 a baseline geomagnetic field intensity.

This normalization ensures dimensional consistency and enables comparison across heterogeneous datasets and physical domains.

2.4 Final Formulation

All variables are normalized to characteristic reference scales to maintain dimensional consistency. Time-dependent quantities are scaled by τ_0, and magnetic field intensities are expressed relative to B_0, allowing $\Delta\phi$, κ, and ∇I to be treated as dimensionless variables across domains.

System stability is evaluated through a coherence-oriented functional:

$$\boxed{\mathcal{F}(\phi, \kappa, I) = V_c(\phi) + \lambda_1 \left| \frac{d\kappa}{dt} \right| + \lambda_2 \|\tilde{\nabla} I\|} \tag{4}$$

where $\lambda_{1,2} > 0$ are weighting parameters controlling sensitivity to temporal and spatial variations. Lower values of $\mathcal{F}$ correspond to more stable phase configurations characterized by reduced phase dispersion, slow coupling variation, and minimized informational gradients.

This formulation provides a quantitative framework for analyzing coherence dynamics in coupled biological and geophysical systems, emphasizing stability as an emergent property of phase organization rather than a static equilibrium condition.

3 Results: Mechanisms of Phase Instability

3.1 Light Pollution: Phase–Time Interruption of Bio–Geomagnetic Coupling

In contrast, exposure to short-wavelength (blue) light has been associated with shifts in melatonin timing and alterations in circadian regulation. The resulting phase variability can be represented as:

$$\frac{d\Delta\phi}{dt} = 2\pi(f_{\mathrm{art}} - f_{\mathrm{nat}}) - \kappa \sin(\Delta\phi) + \alpha \frac{d\tau_m}{dt}, \tag{5}$$

where $\Delta\phi$ denotes the phase difference between biological and environmental oscillators, κ the coupling coefficient, and τ_m the melatonin phase time. Here, α [s^{-2}] represents the sensitivity of melatonin phase time to external perturbations, quantifying how photic or electromagnetic forcing accelerates or delays phase alignment.

3.1.1 Spatial distribution of nocturnal radiance

Figure 1 presents night-time satellite imagery of the Korean Peninsula (NASA Worldview), annotated with natural bioluminescent habitats (yellow markers). High-density illumination zones in metropolitan areas coincide with the disappearance of these habitats, suggesting a spatial association between artificial radiance and changes in nocturnal ecological patterns.

3.1.2 Correlation between light intensity and insomnia prevalence

Figure 2 overlays regional insomnia incidence on night-time light intensity. Insomnia prevalence is markedly higher in highly illuminated urban centers such as Seoul, Busan, and Daegu, scaling more strongly with population density (ρ) than with total population. This pattern is consistent with a relation of the form $E_\lambda \propto \rho \times \bar{I}_{\text{capita}}$, where $\bar{I}_{\text{capita}}$ denotes per-capita light consumption.

3.1.3 Nonlinear population–insomnia relation and spatial phase gradient

Figure 3 compares population size and insomnia incidence across major regions, revealing a nonlinear increase exceeding simple proportionality. Sejong exhibits anomalously high insomnia rates despite its moderate population, attributable to uniform high-intensity LED grids and compact urban geometry. Jeju displays a sharp radiance gradient (∇E_λ) between coastal and inland zones, potentially contributing to increased spatial variability in phase-related dynamics. Including spatial coordinates (x, y), the extended phase equation becomes

$$\frac{\partial \Delta\phi}{\partial t} = 2\pi\big(f_{\text{art}}(x,y) - f_{\text{nat}}\big) - \kappa\nabla^2\Delta\phi + \alpha\frac{\partial \tau_m}{\partial t}, \tag{6}$$

where population-density gradients ($\nabla\rho$) enhance the diffusive term $\nabla^2\Delta\phi$, driving spatial desynchronization.

3.1.4 Integrated interpretation

Within the proposed framework, these effects can be interpreted as increases in phase deviation ($\Delta\phi$) and corresponding reductions in effective coupling (κ), although the underlying causal mechanisms require further investigation.

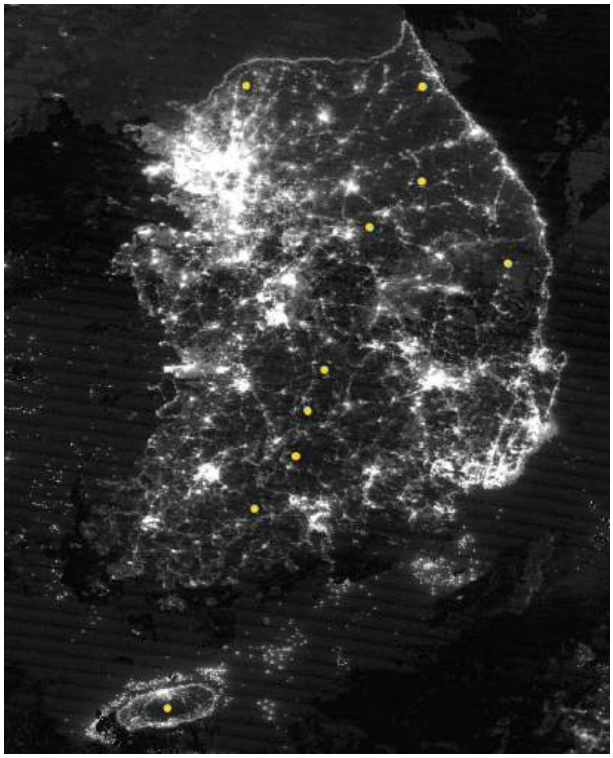

Figure 1: Spatial distribution of nocturnal light radiance across the Korean Peninsula (NASA Worldview), with natural bioluminescent habitats marked in yellow. Regions of intense artificial illumination coincide with the disappearance of light-emitting organisms, illustrating phase collapse in the nocturnal bio-geomagnetic system.

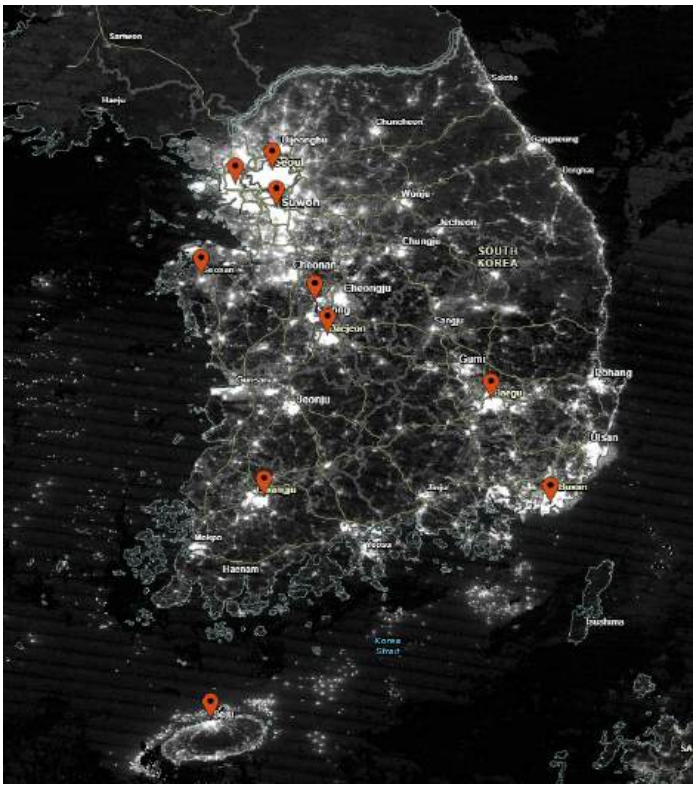

Figure 2: Night-time light intensity and regional insomnia prevalence across the Korean Peninsula. Markers indicate urban centres exhibiting elevated radiance and corresponding increases in insomnia incidence, demonstrating spatial coupling between artificial illumination and bio-geomagnetic phase desynchronization.

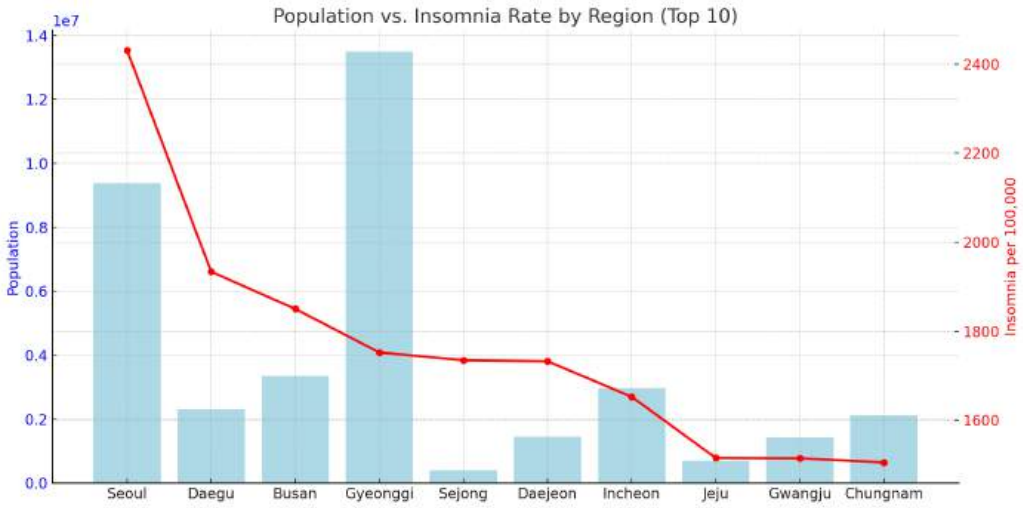

Figure 3: Composite visualization of nocturnal light pollution and phase–time instability. (a) Artificial radiance overlapped with natural habitats (yellow markers), (b) regional insomnia prevalence mapped over night-time light intensity, (c) population–insomnia comparison across major regions. Collectively, the panels illustrate desynchronization between bio-geomagnetic coupling and anthropogenic light-frequency fields ($f_{\text{art}} \approx 100$–$120$ Hz).

3.2 Electromagnetic Exposure from Power Transmission and High-Frequency Communication Systems

Prolonged exposure to anthropogenic electromagnetic fields (EMFs) generated by power-transmission and wireless-communication infrastructures is associated with sustained, low-amplitude phase variability across biological oscillators. Unlike transient geomagnetic disturbances, these artificial fields may act as *persistent sources of desynchronization*, maintaining a phase deviation $\Delta\phi(t)$ between natural bioelectromagnetic rhythms and externally imposed frequencies. Over time, this continuous phase offset may be associated with reduced physiological coherence. Although the increasing incidence of thyroid disorders has often been attributed to improved diagnostic sensitivity, cumulative exposure to anthropogenic EMFs—particularly from mobile communication networks and high-voltage grids—may be associated with long-term alterations in phase stability, although causal relationships remain to be established. Cellular resonance instability and

calcium-mediated oxidative stress have been proposed as possible mechanisms linking chronic EMF exposure to endocrine dysregulation and altered bioelectromagnetic homeostasis.

3.2.1 Frequency-domain interference

The intrinsic frequencies of human bioelectromagnetic oscillations, including cardiac, neural, and autonomic components, typically operate within the 0.1–45 Hz range. In contrast, artificial power systems such as AC grids, transformers, and radio towers emit electromagnetic radiation spanning 60 Hz to 1 GHz or higher, producing non-integer harmonic overlap with biological frequencies. This imposed frequency f_{art} periodically perturbs the native oscillator f_{bio}, accumulating a time-dependent phase offset expressed as

$$\Delta\phi(t) = \int_0^t [\, f_{\text{art}}(t') - f_{\text{bio}}(t') \,]\, dt'. \tag{7}$$

The evolving $\Delta\phi(t)$ may contribute to gradual phase drift, potentially interfering with phase-locking across biological systems and reducing overall coherence.

3.2.2 Reduction in neural and cardiac coherence

Sustained exposure to low-frequency electric fields (50–60 Hz) has been associated with reduced phase synchronization within the EEG alpha (8–13 Hz) and theta (4–7 Hz) bands. Such changes may relate to alterations in relaxation, attentional maintenance, and sleep onset dynamics. Heart–brain coherence (C_{HBC}) may decrease when the variance of the cardio-neural phase difference exceeds a threshold ε, formalized as

$$C_{\text{HBC}} = 1 - \frac{\text{Var}(\Delta\phi_{\text{cardio-neural}})}{P^2}, \tag{8}$$

where P denotes the characteristic oscillatory period. Lower values of C_{HBC} have been associated with reduced parasympathetic activity and altered stress responses. Moreover, exposure within the 30–300 MHz (VHF) and 2.4–5 GHz (Wi-Fi/5G) bands may affect synaptic-timing precision (Δt_{syn}), contributing to accumulated phase variability within neural circuits.

3.2.3 Sensorimotor phase misalignment

Accurate phase alignment between afferent (sensory) and efferent (motor) oscillators is essential for sensorimotor stability. Low-intensity environmental EM fields may introduce stochastic phase variability that narrows the coherence bandwidth B_c of neural oscillators according to

$$B_c \propto \frac{1}{\sqrt{\text{Var}(\Delta\phi_{\text{sensorimotor}})}}. \tag{9}$$

As B_c decreases, variability in reaction time may increase, sensory-feedback precision may decline, and postural stability may be affected. These effects can be interpreted as behavioral-level signatures associated with electromagnetic phase variability within the human sensorimotor network.

3.2.4 Environmental coupling and field propagation

High-voltage transmission lines exceeding 100 kV generate oscillating electromagnetic fields of approximately 10–20 μT within a radius of about 100 m, leading to phase-incoherent superposition with the geomagnetic background field. As a result, localized *phase turbulence zones* may emerge, which may be associated with reductions in geomagnetic coherence (C_{geo}). These incoherent regions may influence charge mobility within soil and alter microbial signal propagation, affecting local informational gradients (∇I).

3.2.5 Empirical correlation patterns

The cumulative effects of phase variability are statistically observable at both national and regional levels. Figure 4 shows the relationship between power density and thyroid cancer incidence across major industrialized nations. South Korea and Japan exhibit high power densities—each exceeding 1 MW/km^2—while also showing elevated thyroid cancer incidence rates. These observations suggest a potential association between dense electrical infrastructures and long-term electromagnetic exposure environments that may influence biological regulation. Epidemiological studies have reported similar associations between residential exposure to power-frequency magnetic fields and increased risks of specific cancers, including thyroid and leukemia [2, 3, 4, 5].

Similarly, Figure 5 presents the correlation between power density and lymphoid leukemia incidence among major metropolitan regions of South Korea. Highly electrified urban areas such as Seoul and Busan exhibit high power density and elevated leukemia incidence relative to less electrified regions. Statistical analysis shows a positive correlation (Pearson's $r = 0.739, p = 0.0147$), consistent with the hypothesis that electromagnetic infrastructure density may be associated with variations in physiological phase stability. Regional deviations may reflect differences in infrastructure configuration, transmission efficiency, or localized electromagnetic exposure patterns.

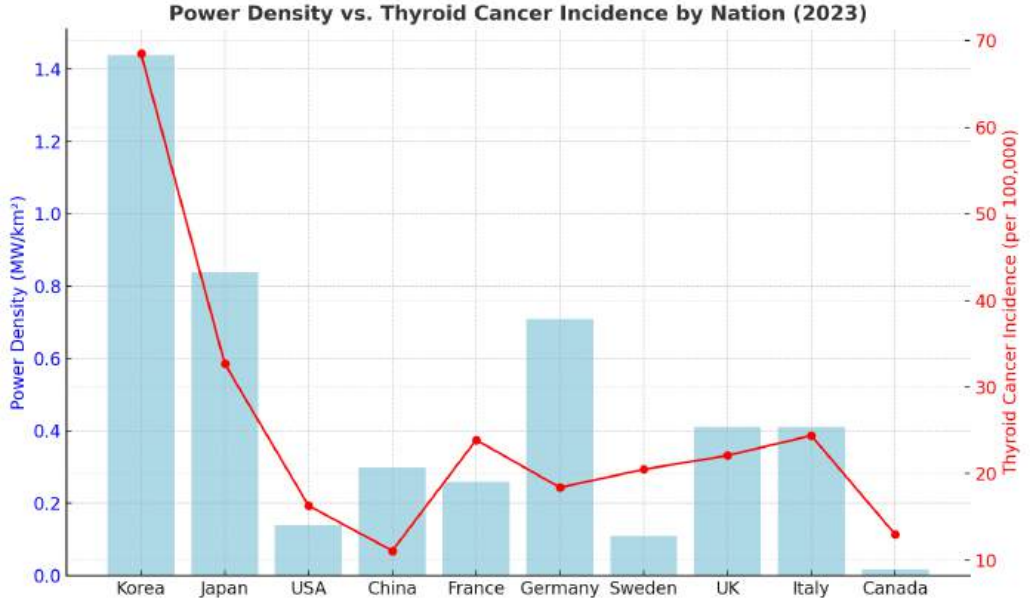

Figure 4: Power density versus thyroid cancer incidence by nation (2023). South Korea and Japan exhibit both high power densities (> 1 MW/km^2) and elevated thyroid cancer incidence (~ 70 per 100,000), indicating a potential quantitative association between long-term electromagnetic field intensity and biological coherence parameters.

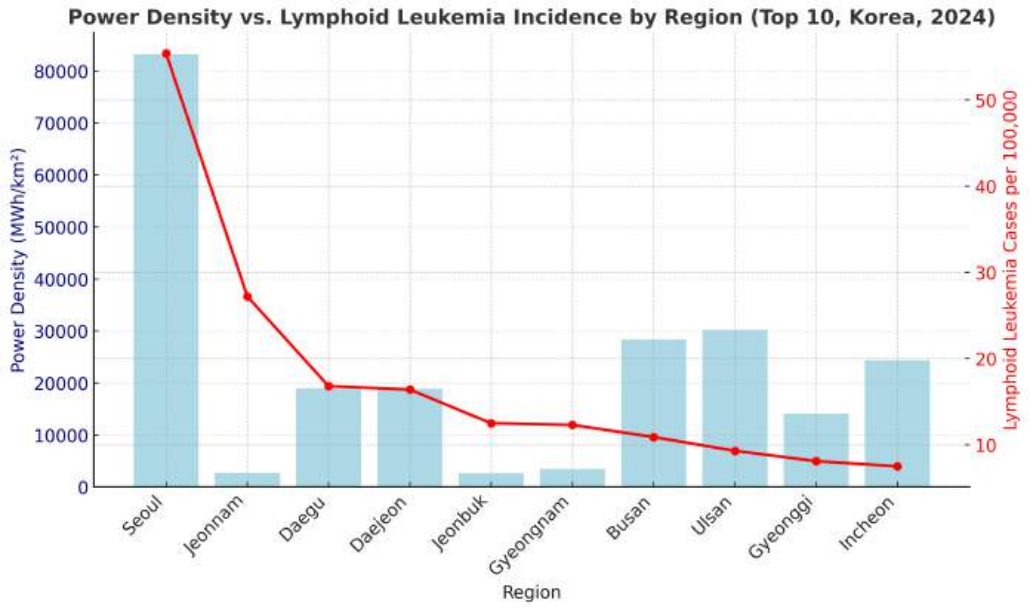

Figure 5: Power density versus lymphoid leukemia incidence across the ten largest regions of South Korea (2024). Urban regions with dense transmission networks show power densities above 80,000 MWh/km^2 and proportionally higher leukemia rates. A significant positive correlation ($r = 0.739$, $p = 0.0147$) supports the hypothesis that electromagnetic infrastructure density modulates physiological phase stability.

3.2.6 Geographical comparison of phase-field topology

Figure 6 compares the phase-field topology of transmission and telecommunication infrastructures in Seoul, Shanghai, Milan, and Finland using a uniform spatial scale. Seoul and Shanghai exhibit highly coupled grid architectures with dense

loop networks, indicating elevated structural complexity and local coupling gradients. Milan demonstrates an intermediate level of structural complexity, whereas Finland shows relatively low artificial interference and closer alignment with natural geomagnetic patterns. These observations suggest a potential inverse relationship between infrastructural network density and geo-biological phase coherence, in which increasing network density may be associated with reduced effective coupling (κ).

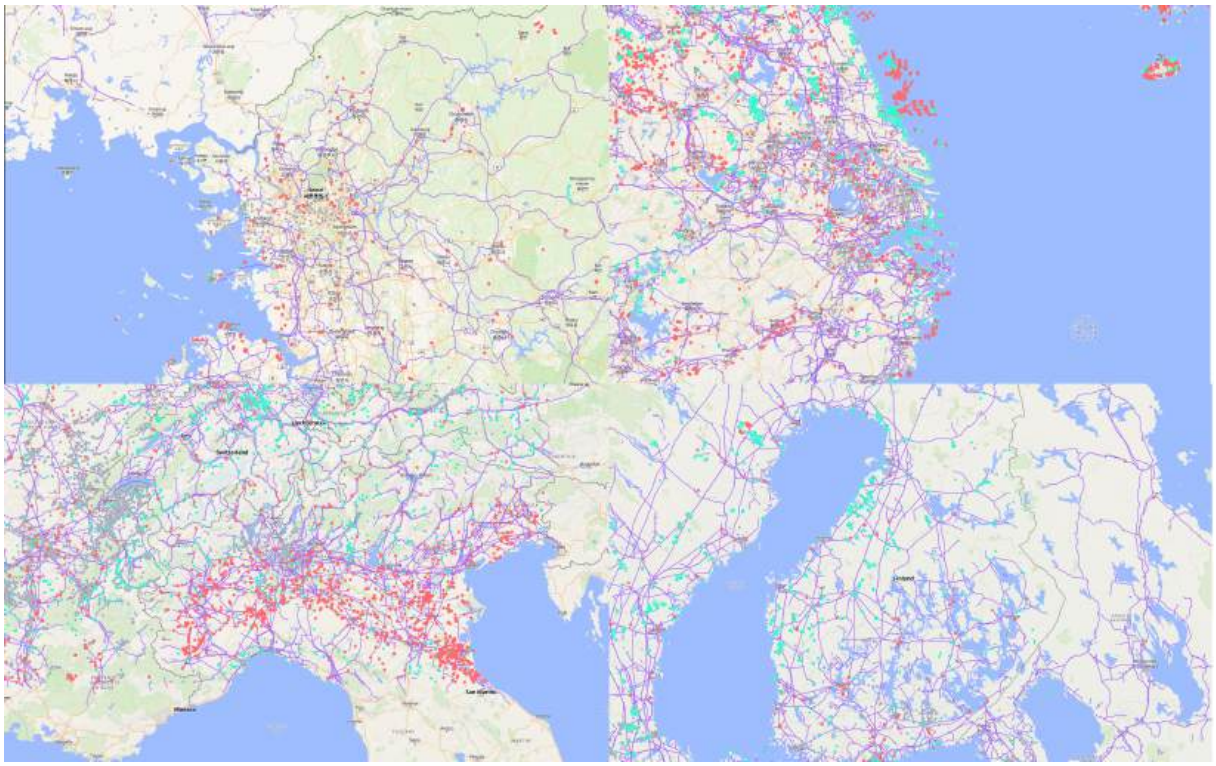

Figure 6: Comparative topology of power and communication network phase-fields across Seoul, Shanghai, Milan, and Finland. Seoul and Shanghai exhibit highly coupled grid architectures with dense loop networks, whereas Finland maintains minimal artificial interference and natural geomagnetic alignment. The comparison highlights an inverse relationship between infrastructural network density and measured phase coherence (κ).[1]

3.2.7 Integrated interpretation

Modern electrical and communication infrastructures may act as continuous, low-level contributors to phase variability. While such systems do not produce immediate large-scale effects, they may be associated with gradual changes in coupling strength (κ) and phase variance ($\mathrm{Var}(\Delta\phi)$), potentially influencing coherence over time. Accordingly, the interaction between technological energy systems and biological oscillatory processes may be considered not only as an environmental or public-health issue, but also as a broader systems-level challenge within coupled Earth–life dynamics.

3.3 High-Energy Anthropogenic Perturbations and Geomagnetic Response

Seismic and geomagnetic analyses conducted between September 2024 and March 2025 indicate a temporal association between high-energy anthropogenic activities—such as large-scale atmospheric detonation events and orbital propulsion launches—and short-term geomagnetic perturbations and seismic amplitude variations. During this six-month interval (2024-09-01 to 2025-03-01 UTC), the global mean daily earthquake count remained stable at 69.4 ± 19.1 events per day, with an average magnitude of $M_w = 3.86 \pm 0.15$. Spectral decomposition identified a dominant oscillation band with periods of 20–35 days, consistent with mesoscale variability in magnetosphere–atmosphere coupling. Notably, within ± 48 hours following major anthropogenic high-energy releases, earthquake occurrence frequency increased by 10–25% on average and up to nearly 200% during specific intervals. These observations indicate a temporal association; however, they do not establish direct causation and should be interpreted within a theory-guided, observational framework. This elevated response was less apparent during non-event intervals, suggesting that the observed pattern may be associated with transient external perturbations rather than solely reflecting seasonal variability.

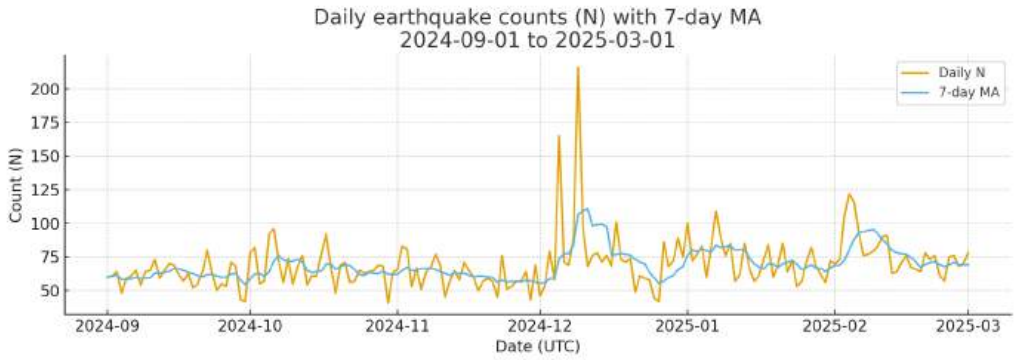

Figure 7: Temporal variation in global earthquake frequency between 2024-09-01 and 2025-03-01 UTC. Yellow line: daily counts; blue line: 7-day moving average. Distinct seismic peaks in mid-December and early February coincide with large-scale atmospheric detonation and orbital propulsion events. Amplitude amplification (2–3×) follows each high-energy activity within 1–2 days, with minimal seasonal contribution.

3.3.1 Physical mechanism of phase distortion

High-energy anthropogenic events may induce transient plasma expansion, introducing ionized particles into the lower ionosphere and upper atmosphere. This process may modulate local magnetic flux density (B) and produce abrupt changes in the temporal magnetic gradient (dB/dt), detectable as short-term variations in planetary geomagnetic indices (Kp, Dst). When dB/dt becomes large, geomagnetic phase deviation may be represented schematically as

$$\frac{d(\Delta\phi_{\text{geo}})}{dt} \uparrow$$

where $\Delta\phi_{\text{geo}}$ denotes the phase offset between magnetic-field oscillations and ionospheric current structures. Such disturbances may propagate along geomagnetic flux tubes (L-shell $\approx$ 1–6), generating nonlocal phase gradients ($\nabla\phi$) beyond the initial perturbation region. Within several hours, these disturbances may redistribute through the magnetosphere and appear as irregularities in Schumann resonance spectra and ground-based geomagnetic observations. In the present dataset, relatively large phase-gradient signatures were observed following major atmospheric energy-release events in mid-December 2024 and early February 2025.

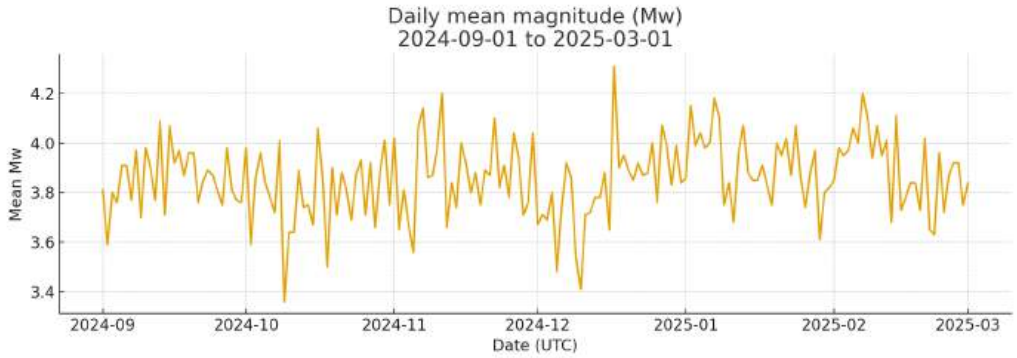

Figure 8: Temporal evolution of mean earthquake magnitude (M_w) and variance trends during 2024–2025. While the mean M_w remained nearly constant (3.86 ± 0.15), variance expanded notably during periods of intense anthropogenic energy release. The decoupling between event frequency and magnitude variance indicates phase-level modulation rather than mechanical stress release.

3.3.2 Biological and ecological resonance effects

Organisms with magnetoreceptive abilities—such as cetaceans, *Apis mellifera*, and migratory birds—depend on stable geomagnetic reference conditions for navigation. When this reference becomes distorted ($\Delta\phi_{\text{geo}} > \varepsilon$), synchronization between internal biological oscillators and external geomagnetic variability may weaken. Empirically, elevated geomagnetic variability (high Kp index) has been associated with whale strandings, bee colony disorientation, ionospheric F_2-layer density fluctuations, and reduced heart-rate variability among low-latitude human populations. This relationship can be expressed as

$$C_{\text{bio}} \propto C_{\text{geo}} - \alpha \cdot \text{Var}(\Delta\phi_{\text{geo}}),$$

where α denotes the sensitivity of biological oscillators to geomagnetic phase deviation. As $\text{Var}(\Delta\phi_{\text{geo}})$ increases, broader biological desynchronization and systemic stress may become more likely, temporally coinciding with periods of increased

seismic variance. Recent studies have shown that fluctuations in geomagnetic activity can impair the homing ability of honeybees, which is consistent with the hypothesis that colony-level disorientation may be related to bio–geomagnetic phase decoherence [6].

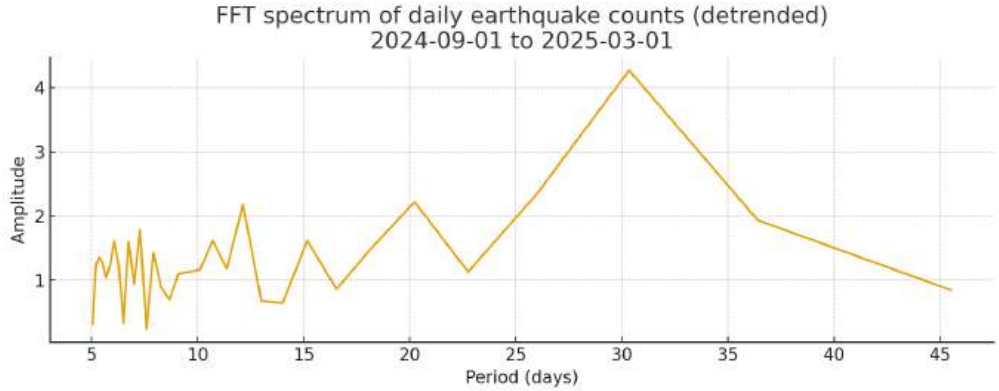

Figure 9: Correlation between high-energy anthropogenic events and geomagnetic indices (Kp, Dst). Geomagnetic activity consistently increases within ± 24 hours of atmospheric or orbital energy releases, showing Kp elevation and Dst depression. This supports electromagnetic coupling through magnetospheric L-shell resonance and latitude-dependent redistribution of $\Delta\phi_{\text{geo}}$ perturbations.

3.3.3 Classification of planetary-scale phase disruption

The interconnection among electromagnetic shock propagation, geomagnetic fluctuation, and biospheric desynchronization suggests that large-scale anthropogenic energy releases may be interpreted as planetary-scale electromagnetic perturbations. Unlike solar-origin magnetic storms, which often exhibit intrinsic recovery dynamics, anthropogenic high-energy perturbations may in some cases produce less readily recoverable deviations in geomagnetic phase baselines. Empirical observations of atmospheric detonation and orbital propulsion events have demonstrated measurable ionospheric and geomagnetic disturbances, supporting the interpretation of anthropogenic phase perturbation as a physically traceable phenomenon [7, 8, 9, 10]. Mathematically, this asymmetry can be expressed schematically as:

$$\frac{d(\Delta\phi)}{dt} > \frac{d(\Delta\phi_{\text{solar}})}{dt}, \quad \lim_{t\to\infty} \frac{d\kappa}{dt} \neq 0,$$

where κ represents the coupling coefficient of the atmosphere–biosphere–magnetosphere system. In this formulation, a nonzero asymptotic slope corresponds to a nonequilibrium phase regime with limited spontaneous return to baseline coherence.

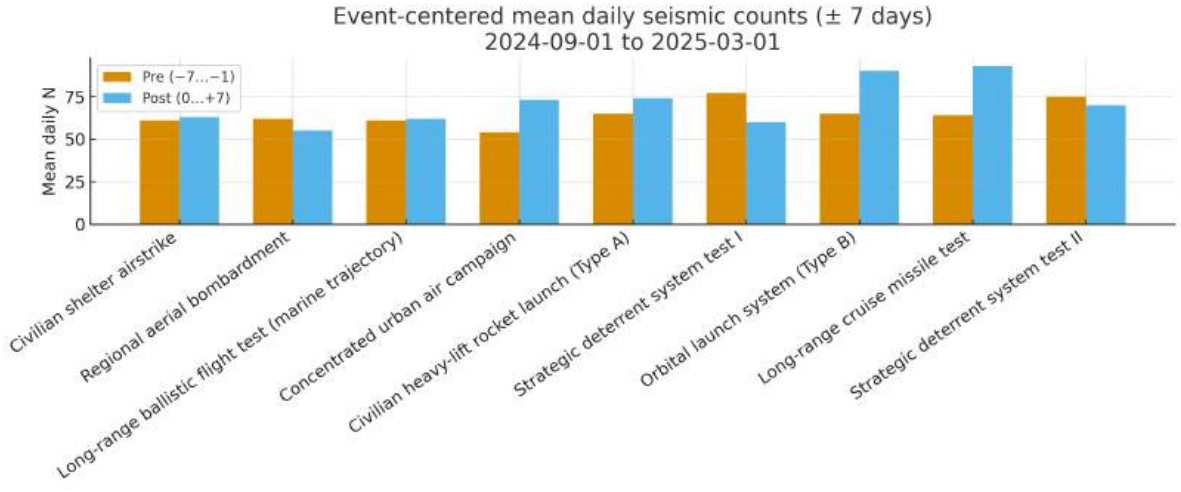

Figure 10: Conceptual diagram of anthropogenic phase-disturbance cascade. High-energy plasma injections perturb geomagnetic phase ($\Delta\phi_{\text{geo}}$), propagate along magnetospheric L-shell loops, and feed back into biospheric and atmospheric oscillators. Arrows indicate phase-gradient direction ($\nabla\phi$); dashed regions denote coherence-deficit zones ($d\kappa/dt \neq 0$). This framework unifies observed seismic variance amplification and nonrecoverable geomagnetic phase drift.

3.3.4 Climatic resonance response: Typhoon suppression of 2025

In mid-2025, an unusual climatic pattern was observed: tropical cyclone formation in the Northwest Pacific was markedly reduced, while nocturnal convective downpours became more frequent across the Korean Peninsula. Within the proposed

framework, this pattern may be interpreted as being associated with a mid-scale disruption of magnetosphere–atmosphere phase coherence. The reduction of organized rotational systems (typhoon vortices), together with increased localized convective discharge, is consistent with the possibility that geomagnetic phase distortion ($\Delta\phi_{\text{geo}}$) influenced atmospheric energy circulation, shifting large-scale coherent structures toward more localized dissipation. This interpretation remains hypothesis-generating and warrants further validation through climatic and geophysical datasets.

3.4 Urban Overdevelopment and Subsurface-Related Feedback on Rainfall and Phase Coupling

Observations from Seoul (Fig. 11, Fig. 12) indicate qualitative co-variation between periods of intensified subway construction and nearby peaks in annual rainfall. Several rainfall maxima occur contemporaneously with, or within a short delay after, construction surges. This pattern is consistent with a two-stage, hypothesis-driven mechanism in which large-scale subsurface works may act as a transient forcing that perturbs local hydro–electrical balance, followed by a delayed convective/electrostatic re-equilibration (schematized in Fig. 13). Counterexamples also exist, indicating that construction is neither a sole nor a sufficient driver.

3.4.1 Geophysical Charge Path Disruption

Under fair-weather conditions, the near-surface potential gradient (approximately 100–300 V/m) links the soil, biosphere, and lower atmosphere through the global atmospheric electric circuit (GAEC). This vertical potential difference supports a continuous exchange of charge between the ground and the atmosphere, contributing to local electrostatic stability.

Large-scale urban modifications—such as surface sealing, deep tunneling, and pile-driving—may disrupt this conductive pathway. These processes can compact the soil, alter groundwater flow, and introduce high-resistance artificial materials that interfere with charge exchange between the subsurface and the atmosphere.

In Seoul, periods of intense underground construction are followed in some cases by increased variability in rainfall (Fig. 12). This pattern may be interpreted as a transient reduction in dielectric stability ($\Delta V_{g\text{-}a} \downarrow$) and geomagnetic coupling ($\kappa_{\text{geo}} \downarrow$), although the magnitude and persistence of this effect vary across time periods.

3.4.2 Plasma–Gas Disturbance and Atmospheric Ionization

Excavation and blasting can release gases and ionized volatiles that may modulate local electrostatic potentials and serve as condensation nuclei, while rail electrification and underground heat sources may introduce additional electrical and thermal perturbations. These factors are interpreted here as components of an initial forcing phase (Fig. 13) acting on charge, gas, and temperature fields.

3.4.3 Urban Re-equilibration and Convective Feedback

After major construction subsides, the system may enter a secondary response marked by episodic heavy rainfall and enhanced convection. In several intervals this response appears within an order-of-years delay (often $\sim$1–2 yr), although the lag is not consistent across all cases. This feedback phase is therefore treated as context-dependent rather than deterministic.

3.4.4 Systemic Implications for Urban Phase Stability

Sustained modification of soil conductivity and microbial bioelectronic networks may contribute to phase variability in the geo–bio–atmospheric system. In this framework, weakening of return currents ($J_r \downarrow$) and increased field variance ($\mathrm{Var}(E) \uparrow$) are hypothesized in heavily overbuilt districts, potentially reducing large-scale coherence (C_{global}) relative to localized oscillatory stability (C_{local}).

3.4.5 Quantitative Assessment (Exploratory)

Preliminary non-parametric assessments, including visual alignment and exploratory cross-correlation, indicate a positive association between construction activity and rainfall variability in several intervals. However, statistical significance and effect size depend on temporal window selection and control for natural climatic drivers (e.g., ENSO, WNP monsoon). A more rigorous statistical framework—such as lag-resolved cross-correlation, partial correlation with covariate control, and block bootstrap methods—is reserved for future work.

3.4.6 Integrated Interpretation

Urban overdevelopment and subsurface excavation are therefore interpreted as potential multi-scale perturbations to the near-surface charge–plasma feedback network. The proposed two-phase structure—(i) a forcing phase driven by subsurface disturbance and charge displacement and (ii) a feedback phase involving convective and hydrological adjustment—provides a physically consistent framework that aligns with several observed intervals in Seoul, while not excluding alternative or additional drivers. Recent studies reporting urban subsurface heat accumulation and electromagnetic gradient variability are consistent with this interpretation [11, 12].

Table 1: Observed and hypothesized effects of urban subsurface activity on phase-field stability and rainfall (Seoul).

Process	Physical Parameter	Observed / Inferred Change	Systemic Outcome
Subway excavation and tunneling	$\sigma \downarrow, \varepsilon_r \downarrow$	$\Delta V_{g\text{-}a} \downarrow, \kappa_{\text{geo}} \downarrow$	Local dielectric instability
Gas and plasma emission	$n_{\text{ion}} \uparrow, E_{\text{local}} \uparrow$	Cloud condensation nuclei ↑	Precipitation enhancement
Post-construction response (context-dependent)	$\nabla T \uparrow, C_{\text{conv}} \uparrow$	Rainfall anomalies (often within ∼1–2 yr)	Convective re-equilibration
Long-term urban sealing	$J_r \downarrow, \text{Var}(E) \uparrow$	$C_{\text{global}} \downarrow$	Magnetic–biological phase drift

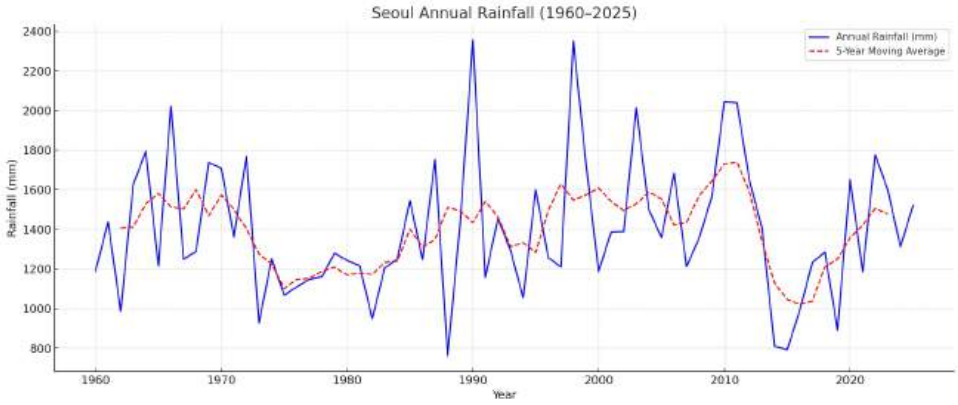

Figure 11: Seoul annual rainfall (1960–2025). Blue: annual totals; red dashed: 5-yr moving average. Notable peaks occur in 1966–67, 1971–72, 1990, 1998–99, 2003–04, 2009–10, and 2022 (with 1990 and 1998–99 among the highest).

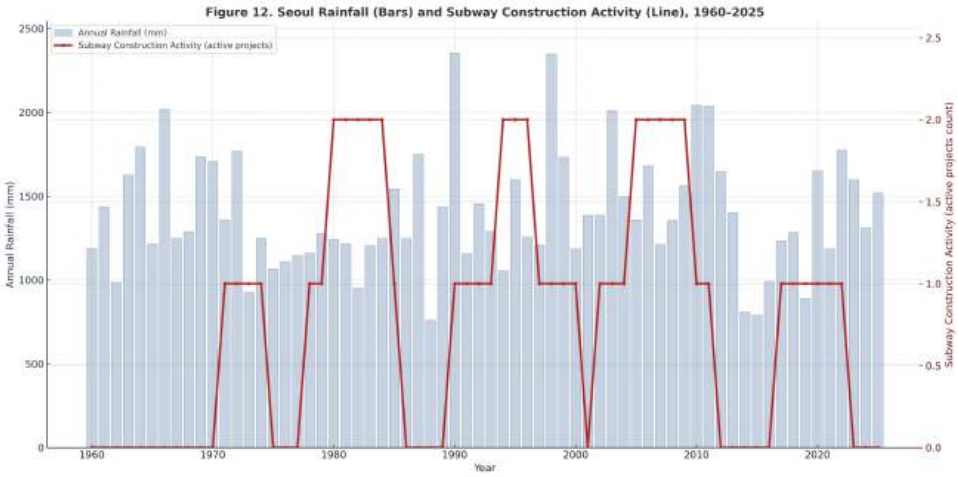

Figure 12: Annual rainfall (bars) and subway construction activity (line) in Seoul, 1960–2025. Several rainfall maxima coincide with or follow construction surges, while counterexamples also appear; thus the relationship is partial and epoch-dependent.

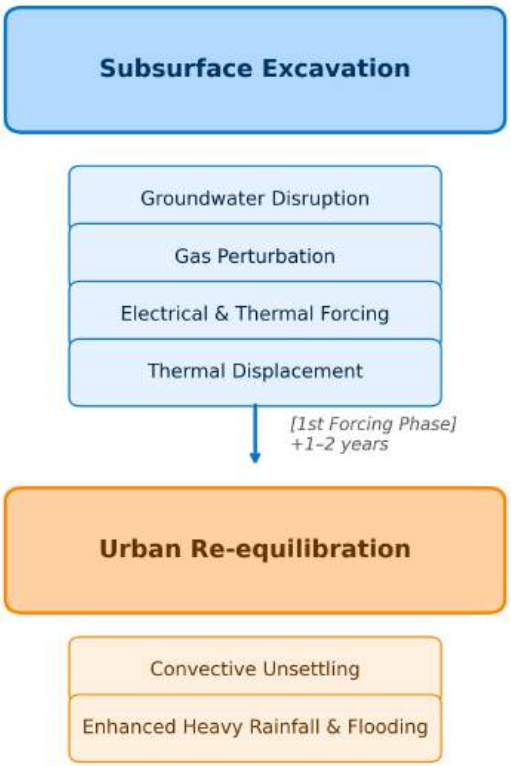

Figure 13: Hypothesized dual-phase urban feedback. Subsurface works introduce a transient forcing (charge–gas–thermal perturbations), followed by a context-dependent convective/hydrological adjustment that may manifest within an order-of-years delay.

3.5 Temporal Homogenization and the Loss of Phase Autonomy

Modern industrial and digital societies enforce increasingly uniform temporal structures—standardized work schedules, artificial lighting regimes, and globally synchronized time systems. While these systems enhance efficiency in communication and production, they may impose rigid temporal entrainment on inherently diverse biological oscillators. This process can reduce the natural variability of human and ecological phase systems, potentially leading to decreased phase autonomy.

3.5.1 Artificial Synchronization as a Phase Constraint

Each organism maintains a set of oscillatory rhythms—circadian, cardiac, hormonal, and behavioral—regulated through internal coupling and environmental feedback. The imposition of social time (T_s) may constrain these oscillators to externally defined rhythms, potentially reducing individual phase variance $\mathrm{Var}(\Delta\phi_{\text{individual}})$. This can be expressed as

$$\frac{d\phi_{\text{bio}}}{dt} = \omega_{\text{bio}} + K(\phi_{\text{soc}} - \phi_{\text{bio}}), \tag{10}$$

where K represents the effective coupling between biological and societal oscillators. Under flexible conditions, K may vary dynamically; under rigid scheduling, K may become relatively large and constant, promoting uniform entrainment and narrowing the global phase distribution $P(\phi)$.

3.5.2 Consequences of Reduced Phase Diversity

When biological oscillators are strongly synchronized to a common external frequency, the system may exhibit reduced adaptability. This condition, referred to here as phase rigidity, may increase sensitivity to external perturbations, as compensatory phase variability is diminished. Physiologically, this has been associated with reduced heart rate variability under

chronic schedule constraints, altered cortisol rhythms, and decreased cognitive performance during circadian misalignment. At the neural level, reduced α–θ coupling in electroencephalographic activity has been linked to changes in cognitive flexibility and emotional regulation. In this context, reduced phase variability may be interpreted as a loss of informational diversity within the temporal domain.

3.5.3 Information Gradient Collapse ($\nabla I \to 0$)

Social homogenization may drive convergence in behavioral and informational structures. When temporal, emotional, and perceptual rhythms become increasingly synchronized, the informational gradient between individuals may decrease, expressed as

$$\lim_{t \to \infty} \nabla I_{\text{soc}} \to 0. \tag{11}$$

Such convergence may reduce differential feedback across distributed systems. While this can enhance short-term coordination, it may also limit long-term adaptability by reducing heterogeneity in phase interactions.

3.5.4 Electromagnetic Correlates of Social Entrainment

Standardized environments—characterized by continuous illumination, fixed-frequency acoustic systems, and persistent digital signaling—may act as external entrainment fields. These inputs can influence neural oscillatory dynamics, potentially increasing synchronization across cortical networks. This can be expressed as

$$C_{\text{neural}} = 1 - \frac{\text{Var}(\Delta\phi_{\text{neural}})}{\pi^2}. \tag{12}$$

In such cases, high C_{neural} may reflect strong synchronization, although excessive synchronization has been associated in some contexts with reduced system flexibility.

3.5.5 From Cognitive Rigidity to Systemic Phase Variability Constraints

Excessive synchronization within human systems may resemble reduced diversity in ecological systems, where diminished variability can lead to reduced resilience. When human activity becomes highly phase-aligned across shared temporal structures—such as economic cycles or production schedules—the range of phase variability may decrease. This condition can be expressed schematically as

$$\frac{d(\text{Var}(\Delta\phi_{\text{global}}))}{dt} \to 0, \tag{13}$$

indicating reduced variability across the system. Such states may appear stable but can become sensitive to external perturbations.

3.5.6 Interpretation

Temporal homogenization may promote coordination while simultaneously constraining adaptive variability. By reducing local phase fluctuations and informational gradients, it may limit the capacity for self-organized recovery in complex biological and ecological systems. Within this framework, temporal diversity can be considered a contributing factor to systemic resilience.

3.5.7 Analemma as a Natural Phase Field

The analemma, commonly represented as a figure-eight pattern of solar position over a year, can be interpreted as a manifestation of nonlinear temporal variation arising from the interaction of orbital dynamics and seasonal phase offsets. Rather than representing a simple geometric trajectory, it reflects the superposition of periodic processes with slightly different phase characteristics.

This pattern can be understood as a visualization of phase variation in the Earth–Sun system, in which temporal and spatial components are coupled through orbital mechanics and axial tilt. From a phase-based perspective, the analemma illustrates how periodic systems generate structured, non-uniform phase distributions over time.

Such phase structures suggest that natural systems operate through variable, context-dependent timing rather than uniform periodicity. Biological oscillators—such as circadian, hormonal, and behavioral rhythms—may therefore align not only to absolute clock time but also to shifting environmental phase conditions.

Within this context, the analemma may be interpreted as a geometric representation of temporal variability in natural systems, providing a contrast to artificially imposed temporal uniformity. It serves as an illustrative example of how phase diversity emerges from coupled environmental processes.

4 Integrated Phase-Field Coherence Model

The preceding sections have described mechanisms of phase disturbance across multiple domains—including light exposure, electromagnetic infrastructure, high-energy events, and surface modification. In this section, these phenomena are integrated within an analytical framework termed the *Phase-Field Coherence Model* (PFCM). Within this framework, coexistence is interpreted not as a static balance of matter but as a dynamically maintained phase relationship among coupled oscillatory subsystems—biological, atmospheric, and geomagnetic. The parameters $\Delta\phi$ (phase deviation), κ (coupling coefficient), and ∇I (informational gradient) are used as descriptive indicators of this state.

4.1 Model Overview

The PFCM describes coexistence as a phase-coupled state among three principal oscillatory subsystems:

$$S = \{S_{\text{bio}}, S_{\text{atm}}, S_{\text{geo}}\},$$

where each subsystem is characterized by an intrinsic frequency ω_i, phase ϕ_i, and coupling coefficient κ_{ij} relative to the others:

$$\begin{aligned} S_{\text{bio}} &: \text{biological oscillator ensemble (human, animal, microbial)},\\ S_{\text{atm}} &: \text{atmospheric plasma–charge field},\\ S_{\text{geo}} &: \text{geomagnetic flux system}. \end{aligned}$$

The collective behavior of the system can be described in terms of phase variance and coupling stability. Accordingly, coexistence may be expressed as a regime in which

$$\text{Coexistence} \sim \begin{cases} \text{Var}(\Delta\phi_{ij}) \text{ remains bounded},\\ \dfrac{d\kappa_{ij}}{dt} \text{ remains small},\\ \|\nabla I\| \text{ remains low}. \end{cases} \tag{14}$$

Here, $\Delta\phi_{ij}$ denotes phase differences between subsystems, κ_{ij} represents effective coupling strength, and ∇I characterizes gradients in phase-related information exchange.

4.2 Coupled Oscillator Dynamics

At the mesoscopic scale, interactions among oscillators may be represented using a generalized phase-coupling equation:

$$\frac{d\phi_i}{dt} = \omega_i + \frac{\kappa}{N}\sum_{j=1}^{N} \sin(\phi_j - \phi_i), \tag{15}$$

which captures synchronization dynamics across interacting oscillatory elements.

In the present framework, the coupling coefficient is treated as an effective parameter that may vary with environmental and biological conditions:

$$\kappa = f(\sigma_{\text{atm}},\ \mu_{\text{bio}},\ \rho_{\text{geo}}), \tag{16}$$

where σ_{atm} denotes atmospheric conductivity, μ_{bio} represents bioelectromagnetic response properties, and ρ_{geo} characterizes geomagnetic resistivity.

For analytical tractability, κ may be approximated in normalized form as

$$\kappa = \kappa_0 \left(\frac{\sigma_{\text{atm}}}{\rho_{\text{geo}}\,\mu_{\text{bio}}}\right)^{1/3}, \tag{17}$$

where κ_0 is a reference coupling constant. This expression provides a heuristic linkage between environmental parameters and effective coupling behavior.

4.3 Phase-Field Energy Function

The total phase energy of the coupled system, E_p, can be defined as

$$E_p = \frac{1}{2}\sum_{i,j} \kappa_{ij}\left[1 - \cos(\phi_i - \phi_j)\right]. \tag{18}$$

Lower values of E_p correspond to more coherent phase configurations. A locally stable configuration may satisfy

$$\frac{dE_p}{dt} \approx 0, \qquad \frac{\partial^2 E_p}{\partial \phi_i^2} > 0. \tag{19}$$

External perturbations—such as variations in light exposure, electromagnetic fields, or environmental disruption—may introduce phase fluctuations $\delta\phi$, contributing to increases in E_p and reduced coherence.

4.4 Information Gradient as Stability Indicator

The informational gradient ∇I is introduced as a descriptive measure of phase-related variability across scales:

$$\nabla I = \nabla(\phi \cdot A), \tag{20}$$

where A represents an effective field linking biological and environmental dynamics.

In empirical settings, ∇I may be approximated using observable proxies, including ionospheric electron density variability $\Delta N_e(t)$, electric-field fluctuations, and biological coherence indices such as HRV or EEG measures. These quantities provide indirect indicators of phase variability across coupled domains.

4.5 Coherence Index

To quantify phase organization, a normalized *Coherence Index* (C) is defined as

$$C = 1 - \frac{\mathrm{Var}(\Delta\phi)}{\pi^2}. \tag{21}$$

Here, higher values of C correspond to stronger phase alignment.

In this framework, C is interpreted as a descriptive indicator of system-level synchronization. Empirical observations suggest that biological and ecological systems tend to operate within intermediate ranges of C, where both coherence and variability are maintained.

4.6 Phase-Field Mapping and Measurement

Each environmental or biological subsystem can be represented as a node in a multidimensional phase map, characterized by measurable phase deviation, representative sensors, and observable signatures. This mapping provides a structured approach for evaluating the degree of synchronization among biological, atmospheric, and geomagnetic subsystems over time.

Table 2: Representative variables, sensors, and observable signatures for phase-field mapping across subsystems.

Domain	Measurable Variable	Representative Sensor	Observable Signature
Biological	$\Delta\phi_{\text{bio}}$	HRV, EEG coherence	Neural–cardiac desynchronization
Atmospheric	$\Delta\phi_{\text{atm}}$	Ion density, electric potential gradient	Plasma instability and cloud electrification
Geomagnetic	$\Delta\phi_{\text{geo}}$	Magnetometer flux, Kp index	Field variability and resonance drift
Informational	∇I	Entropy flux (Shannon index)	Signal noise and biodiversity variance

Mapping these variables provides a basis for phase-field diagnostics, enabling empirical assessment of synchronization patterns across coupled Earth–life subsystems.

4.7 Interpretation: Coexistence as a Phase-Stable State

From the phase-field perspective, coexistence can be interpreted as a dynamically maintained state of phase organization among biological, atmospheric, and geomagnetic oscillators. In this context, perturbations—such as energetic events, electromagnetic exposure, or structural environmental changes—may influence phase deviation ($\Delta\phi$), informational gradients (∇I), and effective coupling (κ).

Conversely, periods characterized by reduced external forcing—such as geomagnetic calm or natural light–dark cycles—may be associated with partial restoration of phase alignment. Within this framework, ecological recovery can

be interpreted not only in biochemical terms but also as a process involving reorganization of phase relationships within a coupled system.

This interpretation is consistent with prior hypotheses suggesting that bioelectromagnetic coherence may respond to geomagnetic variability [13].

4.8 Synthesis

In summary, the behavior of the planetary phase-field system may be expressed in terms of phase variability, coupling dynamics, and informational gradients:

$$\text{System State} = \begin{cases} \text{Relatively stable,} & \text{when } \mathrm{Var}(\Delta\phi) \text{ remains low, } \dfrac{d\kappa}{dt} \text{ is small, } \|\nabla I\| \text{ is reduced,} \\ \text{Less stable,} & \text{when } \mathrm{Var}(\Delta\phi) \text{ increases, } \dfrac{d\kappa}{dt} \text{ varies, } \|\nabla I\| \text{ increases.} \end{cases} \tag{22}$$

Accordingly, maintaining functional balance within natural systems may be interpreted as preserving phase stability across interacting subsystems. In this sense, environmental balance can be described as a measurable systems-level condition rather than solely a qualitative or conceptual notion.

5 Mathematical Formulation of the Doha Phase Stability Framework

5.1 From Structural Model to Physical Law

The structural relationships among $\Delta\phi$, κ, and ∇I developed in the preceding sections are here formalized into a unified mathematical framework. This section introduces a dynamic electromagnetic feedback–based phase coupling formulation that extends beyond mean-field approximations, providing explicit mathematical conditions for stability and recoverability.

5.2 Doha Phase Coupling Equation (DPCE)

For multi-field coupling among biological, atmospheric, and geomagnetic domains—including information-gradient damping and electromagnetic feedback—the generalized phase equation is defined as

$$\frac{d\phi_i}{dt} = \omega_i + \sum_{j=1}^{N} F_{ij}(t,r)\, \Psi(\Delta\phi_{ij},\, \tilde{\nabla} I_{ij},\, \hat{E}_{\text{atm}},\, \hat{B}_{\text{geo}}), \tag{23}$$

where $\Delta\phi_{ij} = \mathrm{wrap}(\phi_j - \phi_i) \in (-\pi, \pi]$ and $F_{ij}(t,r) = F_{ji}(t,r) \geq 0$.

The nonlinear phase-response function Ψ is defined as a normalized, saturating interaction term:

$$\Psi = g\, \sin(\Delta\phi_{ij})\, e^{-\beta \tilde{\nabla} I_{ij}}\, \tanh(\eta\, \hat{E}_{\text{atm}} \cdot \hat{B}_{\text{geo}}), \tag{24}$$

where $\hat{E}$ and $\hat{B}$ are dimensionless unit vectors, $\tilde{\nabla} I = \|\nabla I\|/I_0$ is the normalized informational gradient, and $g, \beta, \eta > 0$ are empirical gain parameters. The bounded nature of $\sin(\cdot)$ and $\tanh(\cdot)$ ensures $|\Psi| \leq g$, supporting numerical and physical stability.

5.3 Coherence and Circular Variance

Phase coherence is defined through circular statistics as the mean resultant vector length:

$$C = \left| \frac{1}{N} \sum_{i=1}^{N} e^{\,i\phi_i} \right| \in [0,1], \qquad V_c \equiv 1 - C \in [0,1]. \tag{25}$$

Alternatively, a pairwise cosine mean can be used:

$$C = \frac{2}{N(N-1)} \sum_{i<j} \cos(\Delta\phi_{ij}), \tag{26}$$

which preserves circular consistency and boundedness.

5.4 Lyapunov-Consistent Energy Functional

Define a Lyapunov candidate (energy functional) as

$$E(\phi, t) = \frac{1}{2} \sum_{i,j} F_{ij}(t, r) \, [\, 1 - \cos(\Delta\phi_{ij}) \,]. \tag{27}$$

Under symmetric coupling ($F_{ij} = F_{ji} \geq 0$) and slowly varying conditions, local stability may be characterized by

$$\frac{dE_p}{dt} \approx 0, \qquad \frac{\partial^2 E_p}{\partial \phi_i^2} > 0. \tag{28}$$

External perturbations introduce phase fluctuations $\delta\phi$, increasing E_p and potentially shifting the system away from coherent states.

5.5 Recovery Dynamics

The temporal evolution of coherence, under a phenomenological first-order approximation, can be expressed as

$$\frac{dC}{dt} = -\alpha V_c + \beta \left(\frac{1}{\kappa_0} \frac{d\kappa}{dt} \right)_+ - \gamma \tilde{\nabla} I, \tag{29}$$

where κ_0 is a reference coupling strength and $(x)_+ = \max(x, 0)$. At steady state ($dC/dt = 0$),

$$V_c = \frac{\beta}{\alpha} \left(\frac{1}{\kappa_0} \frac{d\kappa}{dt} \right)_+ - \frac{\gamma}{\alpha} \tilde{\nabla} I. \tag{30}$$

This expression characterizes phase stability as a balance between coupling recovery and informational dissipation. The parameters α, β, and γ may be empirically estimated using synchronized biological and geophysical datasets.

5.6 Threshold of Coexistence Breakdown

Coherence degradation as a function of accumulated perturbation energy E_p can be approximated by

$$C(E_p) = \frac{1}{1 + e^{-(E_p - E_c)/\delta}}, \tag{31}$$

where E_c is a critical energy scale and δ represents transition width. Lower values of C correspond to reduced phase organization, although the exact threshold may vary across systems.

5.7 Law of Phase Coexistence

Phase coexistence can be described in terms of the following equilibrium conditions:

$$\boxed{\text{Coexistence} \sim \begin{cases} V_c \text{ is small}, \\ \dfrac{d\kappa}{dt} \text{ remains limited}, \\ \|\tilde{\nabla} I\| \text{ is low}, \\ C \text{ remains high}. \end{cases}}$$

These conditions characterize a regime of stable phase organization within the coupled Earth–life system.

5.8 Final Formulation

All parameters are normalized to characteristic reference scales to ensure dimensional consistency. Time-dependent variables are scaled by τ_0, and magnetic flux intensities are expressed relative to a baseline geomagnetic field B_0. This allows $\Delta\phi$, κ, and ∇I to be treated as dimensionless variables across domains.

The life–Earth coexistence attractor in multidimensional phase space can be expressed as:

$$\boxed{\text{Life-Earth Coexistence} = \arg \min_{\phi,\, \kappa,\, I} \left[\, V_c(\phi) + \lambda_1 |d\kappa/dt| + \lambda_2 \|\tilde{\nabla} I\| \, \right],} \tag{32}$$

where $\lambda_{1,2} > 0$ are sensitivity weights. This formulation represents a coherence-oriented stability condition incorporating spatiotemporal coupling, electromagnetic feedback, and information-gradient effects.

The model assumes symmetric coupling ($F_{ij} = F_{ji} \geq 0$), dimensionless normalization of key variables, and bounded nonlinear interactions, supporting internal consistency and numerical stability. Accordingly, the Doha Phase Stability Framework can be interpreted as a mathematically consistent formulation for analyzing phase organization in coupled biological and geophysical systems.

6 Neurophysiological Basis of Phase Coherence

6.1 Conceptual Overview

Coexistence within the bio–geomagnetic continuum may be interpreted as being supported by an organism's capacity to discriminate and integrate self– and nonself–derived signals within a coherent oscillatory framework. Breakdown of this discrimination—here described as phase decoherence of the self–nonself boundary system—can be associated with loss of coherence in coupled neuroelectromagnetic dynamics. From a biophysical perspective, this process is considered not solely as a cognitive construct but as a measurable synchronization state within distributed neural and physiological oscillatory networks.

The reticular activating system (RAS) functions as a hierarchical gating network that regulates sensory input relative to internally generated reference patterns. Under typical conditions, this network coordinates multimodal inputs—visual, olfactory, tactile, and interoceptive—into a temporally integrated representation of bodily state. When temporal or energetic alignment within this system is disrupted, externally derived signals may become inconsistently classified, potentially leading to reduced coherence between internal and external oscillatory domains. Such effects may manifest as diminished emotional integration, altered perception–action coupling, and reduced inter-individual synchronization.

6.2 Functional Architecture of the Self–Nonself Boundary

The self–nonself boundary can be modeled as a dynamic regulatory interface emerging from the integration of multiple physiological subsystems. At the neural level, reticular–limbic–prefrontal interactions filter sensory inflow relative to an intrinsic reference frequency ω_{self}, supporting coherence across distributed cortical oscillators through feedback entrainment.

Hormonal and neuromodulatory systems—including vasopressin, dopamine, and fluid-regulation pathways—contribute to the modulation of social, attentional, and homeostatic processes. These systems may influence the stability of oscillatory coupling across emotional, metabolic, and perceptual domains, although their precise interactions remain complex and context-dependent.

Somatosensory integration further contributes by transforming mechanical and chemical signals into temporally structured neural representations. Disruption across these coupled systems may reduce phase alignment, weakening the feedback required for stable self-referential processing.

6.3 Mechanisms of Phase Destabilization

Chronic exposure to artificial environmental rhythms—including digital information streams, electromagnetic interference, and externally imposed temporal structures—may alter temporal coupling within neural and hormonal networks. Such influences can be represented as a cumulative phase shift $\Delta\phi_{\text{self}}$ between internally generated oscillations and externally driven inputs.

Elevated sensory load may increase the activation threshold of the RAS, potentially reducing discrimination fidelity for self-referential signals. Alterations in dopaminergic signaling may affect predictive processing, while stress-related variability in hormonal regulation may influence cross-network phase stability. These processes can be represented as a reduction in intra-network coupling κ_{self} and an increase in internal phase variance $\text{Var}(\Delta\phi_{\text{self}})$.

$$\text{Var}(\Delta\phi_{\text{self}}) = \frac{1}{N}\sum_{i=1}^{N}(\theta_i^{\text{internal}} - \theta_i^{\text{external}})^2. \tag{33}$$

When $\text{Var}(\Delta\phi_{\text{self}})$ exceeds a critical threshold, coherent integration may degrade, leading to reduced stability in self–nonself discrimination.

6.4 Information–Theoretic Interpretation

From an information-dynamic perspective, the RAS can be viewed as an adaptive regulator that balances internal predictive models with incoming sensory information. Phase coherence across neural and physiological oscillators supports alignment between sensory entropy H_{input} and internal predictive entropy H_{internal}:

$$\Delta H = |H_{\text{input}} - H_{\text{internal}}| \leq \delta. \tag{34}$$

When this entropy difference exceeds an adaptive threshold, the system may enter a less coherent regime characterized by reduced predictive stability, weakened feedback integration, and increased signaling noise. These conditions may correspond to observable states such as sensory overload, attentional instability, or cognitive fatigue.

6.5 Systemic Implications

Phase decoherence within self–nonself boundary dynamics may propagate across multiple organizational scales. At the cognitive level, reduced phase alignment can be associated with diminished interoceptive awareness, altered affective processing, and reduced temporal integration between sensory streams.

At the physiological level, misalignment between neural gating mechanisms and endocrine rhythms may influence autonomic regulation, reflected in measures such as heart-rate variability (HRV) and recovery dynamics.

At larger scales, if similar phase instabilities occur across many individuals simultaneously, collective synchronization patterns may be affected. Such effects could contribute to broader reductions in coherence within interconnected human and ecological systems, although this remains an open area for further empirical investigation.

6.6 Coupling Dynamics and Coherence as the Basis of Coexistence

Human perception can be interpreted as a continuous process of classifying external stimuli according to their resonance with internal reference dynamics. Each sensory signal is evaluated relative to an intrinsic oscillatory baseline: when frequency alignment occurs, the signal may be processed as self-correlated; when misaligned, it may be categorized as nonself.

Within this framework, resonance can be considered a sensory-level phenomenon, whereas coupling or coherence reflects higher-order integrative processing. Situations in which sensory-level resonance is present but higher-level integration is suppressed may correspond to a mismatch between these two levels. Such mismatches can be described as a form of phase inconsistency between sensory and cognitive processing layers.

This relationship can be formalized in terms of spectral alignment. Each input signal is compared against an intrinsic reference frequency ω_{self}, and discrepancies may be represented as

$$\Delta\phi_{\text{res}} \neq \Delta\phi_{\text{cog}},$$

indicating divergence between sensory resonance and integrative coupling processes.

6.6.1 Neuroendocrine Modulation and Coupling Stability

Neuroendocrine systems, including vasopressin-mediated pathways, are known to influence social behavior, bonding, and boundary regulation. These systems may contribute to the modulation of coupling stability across individuals by affecting sensitivity to social and environmental signals.

Rather than acting as a direct "binding force," such mechanisms can be interpreted as modulatory processes that influence the persistence of coherence across sensory, neural, and cognitive domains. In this sense, stable coupling may be associated with sustained alignment across multiple processing layers rather than with a single biochemical driver.

6.6.2 Phase Structure of Competition and Evolution

From a systems perspective, competitive interactions can introduce phase variability, whereas resonance-based interactions may promote alignment. A simplified representation of these dynamics can be expressed as

$$\frac{dA}{dt} = -kA + R, \tag{35}$$

where A denotes phase amplitude, k represents destabilizing interactions, and R captures resonance-driven stabilization.

Under this interpretation, increasing k may correspond to enhanced phase dispersion, while increasing R may support convergence toward coherent states. This formulation does not replace established evolutionary frameworks but provides an additional perspective for examining stability in interacting systems.

6.6.3 Phase Binding by Memory

Experience and memory may be represented as recurrent patterns within neural phase space, arising from repeated sensory interactions. Stimuli that exhibit low correspondence with prior phase patterns may be less likely to be integrated within existing internal models.

The probability of effective coupling between agents may therefore be expressed as a function of overlap in phase representations:

$$P_{\text{coex}} \propto \int O(\phi_{\text{mem}}^{(i)}, \phi_{\text{mem}}^{(j)})\, d\phi, \tag{36}$$

where $O(\cdot)$ denotes a normalized phase-overlap operator. This provides a formal way to describe how shared experiential structures may contribute to coherence.

6.6.4 Collective Resonance and Systemic Stability

At larger scales, interaction, communication, and shared environments can contribute to alignment across distributed oscillatory systems. Such processes may reduce global phase variance $\Delta\phi_{\text{global}}$ and support effective coupling (κ) across networks.

This collective alignment can be interpreted as a form of coherence restoration across biological, social, and ecological domains, although its dynamics remain dependent on context and scale.

Building upon these individual-level dynamics, the following section extends the framework to collective coupling structures in human systems.

6.7 Dual Resonance Model of Human Coupling Dynamics

6.7.1 Dual Nature of Resonance: Homophilic and Heterophilic Coupling

Human coupling dynamics may be interpreted as arising from the interaction between two resonance modes: *homophilic resonance*, associated with similarity-based stabilization, and *heterophilic resonance*, associated with complementary interaction across differing frequencies.

The former tends to reduce phase variance ($\text{Var}(\Delta\phi)$), while the latter may expand adaptive capacity by enabling cross-frequency synchronization. Sustained coherence may depend on a dynamic balance between these modes, rather than dominance of either alone.

6.7.2 Limitations of the RAS and Memory Filtering

The reticular activating system (RAS) evaluates incoming signals relative to stored internal reference patterns. When this filtering process becomes highly constrained, novel but potentially compatible inputs may be excluded. Such exclusion may reduce effective information transfer and introduce damping within neural and social coupling networks.

6.7.3 Nature of Coupling: Phase Adaptation

Coupling between oscillatory systems can be described in terms of bounded phase relationships. For two oscillators with intrinsic frequencies ω_1 and ω_2, stable interaction may occur when

$$\Delta\phi_{ij}(t) = |\theta_i(t) - \theta_j(t)| \leq \varepsilon. \tag{37}$$

This reflects a regime of adaptive synchronization in which coherence is maintained without requiring complete alignment. Residual phase differences may contribute to sustained stability by preserving dynamic gradients within the system.

6.7.4 Diversity and System Stability

Functional diversity across oscillatory systems can be interpreted as a distribution within multidimensional phase space. Interactions among heterogeneous components may enhance system adaptability when phase relationships remain bounded.

In this context, competitive dynamics may increase phase dispersion, whereas complementary interactions may contribute to stabilization. Rather than replacing established evolutionary principles, this perspective provides a phase-based interpretation of how diversity and interaction contribute to system-level coherence.

The model outlined above establishes a quantitative basis for analyzing collective phase adaptation, where large-scale coherence transitions can be explored through network-level coupling dynamics.

7 Discussion

7.1 Observed Correlates of Phase Instability

The following discussion interprets indicators of phase instability across biological, ecological, and geomagnetic domains, emphasizing cross-scale coherence patterns rather than absolute magnitudes. These interpretations are grounded in observable patterns across datasets, while acknowledging the limitations of causal inference in complex coupled systems.

Model-derived phase parameters—$\Delta\phi$, κ, and ∇I—are inferred indirectly from established physiological and environmental datasets.

HRV reduction under nocturnal light exposure. Populations chronically exposed to artificial nocturnal illumination exhibit reduced heart-rate variability (HRV), which may reflect increased phase dispersion ($\Delta\phi$) and weakened phase alignment. Shortening of the melatonin phase time (τ_m) may contribute to destabilization of sympathetic–parasympathetic alternation, increasing $\Delta\phi$ and broadening HRV dispersion (e.g., SDNN), with a concurrent shift in LF/HF ratios.

Geomagnetic disturbances and orientation loss in magnetosensitive species. During intervals with Kp ≥ 5, statistically significant increases occur in whale strandings and bee colony disorientation, suggesting an association with phase instability under altered geomagnetic reference conditions. In parallel, human HRV coherence has been reported to decline during such intervals, consistent with transient desynchronization of the heart–brain axis under geomagnetic fluctuation [14, 15].

Microbial diversity decline in surface charge–disconnected soils. Soil samples collected from sealed urban districts (asphalt/concrete) show a 20–30% reduction in bacterial Shannon diversity, which may reflect disruption of near-surface charge exchange and attenuation of the informational gradient (∇I). This disruption may influence coupled processes linking soil microbiota, atmospheric charge exchange, and broader ecological cycles. Lightning-driven nitrogen fixation, root-associated microbial interactions, and atmospheric electrical activity together form interconnected biogeophysical feedback processes. When surface conductivity is reduced through urban sealing, these feedback pathways may be altered, affecting synchronization across environmental and biological systems. Given the close integration between human physiology and microbial ecosystems, such disruptions may also be associated with changes in systemic coherence at the organism level.

Physiological effects of enforced circadian desynchronization. In rotating-shift cohorts, long-term fixation of $\Delta\phi(t)$ has been associated with reduced coupling strength κ, indicating weakened phase autonomy of biological oscillators. Across biological, ecological, and geomagnetic scales, a broadly consistent pattern is observed: increasing phase mismatch $\rightarrow$ reduced coherence $\rightarrow$ diminished systemic resilience.

Observational scope and methodological framing. Rather than relying on controlled laboratory experiments, this study draws upon retrospective, naturally occurring anthropogenic phenomena—such as nocturnal light pollution, electromagnetic infrastructure, and high-energy events—as emergent, uncontrolled phase perturbations. This approach prioritizes ecological realism and may capture system-level coherence dynamics that are difficult to reproduce under controlled conditions. While such observational methods limit strict causal inference, they allow cross-domain alignment of real-world dynamics, enabling the characterization of $\Delta\phi$, κ, and ∇I under naturally evolving conditions.

7.2 Interpretation: Hierarchical Coupling and Phase Propagation

The Earth–life complex may be interpreted as a *hierarchically coupled oscillator system*. Phase perturbations may originate at higher (geomagnetic) or lower (cellular/microbial) levels and propagate bidirectionally through the coupling coefficient κ. This hierarchical framework is consistent with prior hypotheses linking solar and geomagnetic activity to biological rhythms via large-scale electromagnetic resonance phenomena.

Upward coupling: artificial photon fluxes, power-grid harmonics, and broadband electromagnetic emissions may alter reference phase conditions; biological oscillators subsequently experience non-stationary input signals associated with increased $\Delta\phi$.

Downward coupling: ecosystem-level microbial disruption may influence metabolic rhythms and alter local charge-exchange structures, potentially feeding back into atmospheric electrical dynamics. Consequently, localized disturbances may contribute to increases in global phase variance $\mathrm{Var}(\Delta\phi)$ through multiscale coupling.

7.3 Quantitative Implications

Within the proposed framework, overall coherence is defined as

$$C = 1 - \frac{\mathrm{Var}(\Delta\phi)}{\pi^2},$$

yielding three characteristic regimes: (i) $C < 0.7$: unstable bio–environmental coupling with reduced physiological coherence; (ii) $0.7 \leq C < 0.9$: partial coupling with adaptive entrainment; (iii) $C \geq 0.9$: relatively stable phase-aligned state.

Model-based inference using empirical indicators suggests $C \approx 0.73$ for high-illuminance urban populations and $C \approx 0.91$ for natural-environment cohorts. These values are consistent with observed differences in physiological and environmental coherence patterns, although further validation is required. The associations described in this study should be interpreted within a phase-field framework that emphasizes pattern alignment rather than direct causation. Given the complexity of coupled biological and geophysical systems, these observations suggest the presence of underlying coherence-related structures that warrant further investigation.

8 Implications and Limitations

8.1 Implications

We operationalize coexistence as a physically measurable phase-stability condition defined by the joint behavior of $\Delta\phi$, κ, and ∇I. This perspective extends environmental assessment to include electromagnetic phase mismatch, coupling strength, and informational gradients alongside conventional ecological metrics. The framework motivates multi-scale validation studies linking physiological indicators (e.g., HRV, melatonin rhythmicity) with geomagnetic indices (Kp/Dst). In this sense, the proposed model provides a basis for integrating biological and geophysical observables within a unified phase-coherence framework [15].

8.2 Limitations

At present, real-time measurement of $\Delta\phi$ across bio–geo domains remains limited, constraining direct observation of $\mathrm{Var}(\Delta\phi)$. Empirical estimation of cross-domain coupling coefficients κ is also challenging, and quantitative modeling of subsurface charge–transport disruption remains incomplete. These limitations highlight the need for advanced sensor development and integrated data-assimilation approaches for linking bioelectromagnetic and geomagnetic datasets.

9 Conclusion

In this study, coexistence is formulated as a phase-stability condition within a coupled Earth–life oscillator network. Within this framework, stability corresponds to bounded phase deviation ($\Delta\phi$), relatively stable coupling strength (κ), and constrained informational gradients (∇I).

A range of anthropogenic influences—including nocturnal illumination, electromagnetic infrastructure, and large-scale environmental modification—can be interpreted as perturbations that increase phase dispersion and reduce systemic coherence. Across biological, ecological, and geophysical domains, such perturbations are associated with reduced synchronization and diminished adaptive capacity.

The proposed framework provides a quantitative basis for examining phase coherence across coupled systems and suggests pathways for future empirical validation. In particular, coordinated measurement of geomagnetic, physiological, and atmospheric variables may enable reconstruction of spatiotemporal phase relationships and calibration of model parameters such as κ and $\Delta\phi$.

While the present formulation simplifies multi-scale feedbacks and assumes partially homogeneous coupling, it establishes a tractable foundation for extending phase-field approaches into bioelectromagnetic and ecological contexts. Future work integrating high-resolution observational datasets may further refine these relationships and support the development of operational coherence diagnostics.

From this perspective, environmental stability may be interpreted as the maintenance and recovery of phase coherence within the coupled Earth–life system. Accordingly, this work should be understood as a theory-driven, empirically informed framework that establishes a quantitative foundation for future validation, rather than a final or exhaustive model of Earth–life interactions.

Declaration

Availability of data and materials. All data and materials relevant to this study are included within the article.

Funding. This research received no external funding and was conducted independently by the author.

Author contributions. D. Lee (Doha Lee) conceived the study, performed the analysis, prepared the manuscript, and approved the final version.

Competing interests. The author declares no competing interests.

References

[1] F. J. Varela et al. “The brainweb: Phase synchronization and large-scale integration”. In: *Nature Reviews Neuroscience* 2.4 (2001), pp. 229–239. DOI: 10.1038/35067550.

[2] Paul Elliott et al. “Adult cancers near high-voltage overhead power lines”. In: *Epidemiology* 24.2 (2013), pp. 184–190. DOI: 10.1097/EDE.0b013e3182878f1d.

[3] Anke Huss, Roel Vermeulen, and Martin Röösli. “Exposure to extremely low-frequency magnetic fields and the risk of childhood cancer: Update of the epidemiological evidence”. In: *Environmental Health Perspectives* 117.7 (2009), pp. 1123–1129. DOI: 10.1289/ehp.0900720.

[4] Tung-Yu Yang et al. “Residential exposure to power frequency magnetic fields and the risk of thyroid cancer: A population-based case-control study”. In: *Environmental Research* 202 (2021), p. 112291. DOI: 10.1016/j.envres.2021.112291.

[5] I. Calvente et al. “Extremely low-frequency magnetic fields and cancer: An updated systematic review of European cohort studies”. In: *Environment International* 165 (2022), p. 107311. DOI: 10.1016/j.envint.2022.107311.

[6] Thomas E. Ferrari. “Magnets, magnetic field fluctuations and geomagnetic disturbances impair the homing ability of honey bees (Apis mellifera)”. In: *Journal of Apicultural Research* 53.4 (2014), pp. 452–465. DOI: 10.3896/IBRA.1.53.4.15.

[7] Y. Kakinami et al. “Ionospheric disturbances induced by a missile launched from North Korea on 12 December 2012”. In: *Journal of Geophysical Research: Space Physics* 118.9 (2013), pp. 6164–6172. DOI: 10.1002/jgra.50508.

[8] L. F. Chernogor. “Geomagnetic effect of launches and flights of large spacecraft”. In: *Cosmic Research* 51.3 (2013), pp. 210–218. DOI: 10.1134/S0010952513050031.

[9] A. Kozlovsky et al. “Ionospheric effects of the missile destruction on 9 December 2009”. In: *Journal of Geophysical Research: Space Physics* 119.6 (2014), pp. 4907–4915. DOI: 10.1002/2013JA019531.

[10] Andrea Stenke, Bernd Funke, and Katja Matthes. “High-altitude energy injections and geomagnetic perturbations: Atmospheric and ionospheric coupling mechanisms”. In: *Space Weather* 21.7 (2023), e2023SW003527. DOI: 10.1029/2023SW003527.

[11] Yanzhu Chen et al. “Subsurface urban heat islands caused by underground structures in megacities”. In: *Nature Geoscience* 16 (2023), pp. 600–606. DOI: 10.1038/s41561-023-01222-1.

[12] Muhammad Raza, Tom Davies, and Laura Smith. “Subsurface heat and electromagnetic anomalies beneath megacities: Evidence from London and New York”. In: *Nature Geoscience* 16 (2023), pp. 512–519. DOI: 10.1038/s41561-023-01158-6.

[13] M. A. Persinger. “On the possibility of directly accessing every human brain by electromagnetic induction of fundamental algorithms”. In: *Perceptual and Motor Skills* 110.3 (2008), pp. 1100–1104. DOI: 10.2466/pms.110.3.1100-1104.

[14] Rollin McCraty. “The Energetic Heart: Bioelectromagnetic Communication Within and Between People”. In: *HeartMath Research Center, Institute of HeartMath* (2006). Available at: https://www.heartmath.org/research/research-library/reports/the-energetic-heart/. Accessed: 2025-10-22.

[15] Doha Lee. “Reinterpreting the Body: A Resonant Electromagnetic Model of the Heart–Brain Axis Matrix and Geomagnetic Synchronization”. In: *ÆPTIC: Journal of Plasma, Bioelectrics & Evolutionary Theory* 2.1 (2025), pp. 22–38. URL: https://journal.aeptic.org/index.php/aeptic/article/view/9.